Tuning characteristics of mirrorlike T-shape terahertz metamaterial using out-of-plane actuated cantilevers

Yu-Sheng Lin and Chengkuo Lee

Citation: Applied Physics Letters **104**, 251914 (2014); doi: 10.1063/1.4885839
View online: http://dx.doi.org/10.1063/1.4885839
View Table of Contents: http://scitation.aip.org/content/aip/journal/apl/104/25?ver=pdfcov
Published by the AIP Publishing

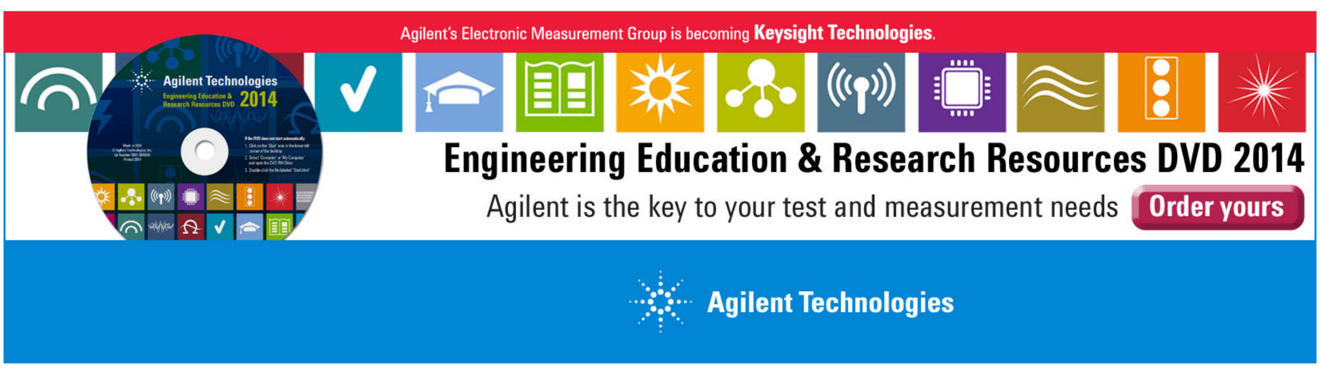

APPLIED PHYSICS LETTERS **104**, 251914 (2014)

Tuning characteristics of mirrorlike T-shape terahertz metamaterial using out-of-plane actuated cantilevers

Yu-Sheng Lin and Chengkuo Lee[a)]

Department of Electrical and Computer Engineering, National University of Singapore, 4 Engineering Drive 3, Singapore, Singapore 117581

(Received 15 January 2014; accepted 12 June 2014; published online 26 June 2014)

We present a mirrorlike T-shape metamaterial (MTM) with out-of-plane movable microstructures for enabling active tuning of resonant frequency in the terahertz (THz) region. The resonant frequency of MTM device can be actively controlled by using either electrostatic force or liquid force. First, by gradually increasing the bias, the cantilevers were continuously deformed towards the substrate and then completely snapped down when the bias reached the critical pull-in voltage (12 V). The tuning range is 0.50 THz as compared to the device without driving voltage to that operated at the pull-in voltage. Meanwhile, we dropped different liquids on the snap-down device surface. In the case of device covered with deionised water, the resonant frequency shift of 0.17 and 0.21 THz were measured for inductive-capacitive and dipolar resonances, respectively. Furthermore, we also demonstrate the flow tuning capability of MTM device integrated with a polydimethylsiloxane fluidic channel by using different injection flow rate from 0 to 5 ml/min. The tunability of MTM device is 0.30 THz due to the different bending states of the MTM cantilevers under different liquid forces. © *2014 AIP Publishing LLC*. [http://dx.doi.org/10.1063/1.4885839]

Recently, terahertz (THz) metamaterials have received tremendous attention owing to their ability to exhibit strong electric and magnetic responses to manipulate the amplitude, direction, polarization, wavelength, and phase of electromagnetic (EM) waves.[1,2] The EM response of the metamaterial can be actively controlled through external stimulus, which is of great significance in real time applications.[2] To increase the interaction of the THz field with the sample, research has been carried out in this field to characterize how these THz waves interact with materials for numerous potential applications such as invisibility cloaking devices,[3] high-resolution superlenses,[4] and perfect absorber.[5]

The tunability of metamaterials has attracted intense research interest, since the active control of metamaterials characteristics is necessary to provide a flexible and versatile platform for mimicking fundamental physical effects. The typical tuning methods have been implemented by means of semiconductor diodes,[6,7] or by changing the surrounding media such as electrical effects in liquid crystals,[8,9] thermal control,[10–13] ferroelectric materials,[14] laser light illuminating,[15–17] and magnetostatic fluid.[18] However, these tuning methods are passive control of the metamaterials properties, highly dependent on the nonlinear properties of the material used, and also limit the tuning range. Alternatively, structural tunability is a straightforward way to control the EM properties of the metamaterials structures. Micro-electro-mechanical techniques are well developed for the realization of movable microstructures. Among these techniques, electrostatic force is usually to be utilized for changing the in-plane gap of metamaterial structures[19–22] or deforming the structural layout.[23–28] Another technique is used the electrothermal actuation mechanism to adjust the metamaterial structures.[29,30]

In this Letter, we present a mirrorlike T-shape metamaterial (MTM) with active and continuous out-of-plane control of resonant frequency by using either electrostatic force or liquid force. First, MTM device can be an optical THz filter by using electrostatic force. When the device is on snap-down state at pull-in voltage that can be used as a refractive index sensor when we dropped different kinds of liquids on the device surface. We then monitored the changes in the transmission as the device was filled with various liquids, namely, nitrogen (N_2) ($n = 1.00$), acetone ($n = 1.36$), isopropyl alcohol (IPA) ($n = 1.37$), ethanol ($n = 1.60$), and deionised (DI) water ($n = 2.10$). These liquids give a good spread of refractive index values, enabling us to investigate the efficacy of THz sensing with various aqueous samples. Furthermore, MTM device was encapsulated in a polydimethylsiloxane (PDMS) bonded structure to form a fluidic channel. In order to explore the flow tuning characteristics, the external liquid can be controlled with different flow rates driven by a syringe pump through the MTM surface. All the EM responses of device were characterized by using THz time domain spectroscopy (THz-TDS, TeraView TPS 3000) in transmission mode, included the device actuated by two actuation mechanisms, i.e., electrostatic force and liquid force, and the device covered with various liquids.

Figure 1(a) shows the schematic of the proposed MTM device with released cantilevers. It consists of mirrorlike T-shape cantilevers with a period of 104 μm. The compositions of device are $Al/Al_2O_3/SiO_2$ with 500/20/100-nm thicknesses deposited and patterned on silicon wafer, respectively. The detailed fabrication process flow can be referred to our previous results.[24] The EM tunability of device is achieved by incorporating flexible T-shape cantilevers with a gap that can be actuated by electrostatic force. The series capacitance of the T-shape cantilevers will depend on the position or bending of the cantilever. Figure 1(b) shows the SEM image of the

[a)]Author to whom correspondence should be addressed. Electronic mail: elelc@nus.edu.sg

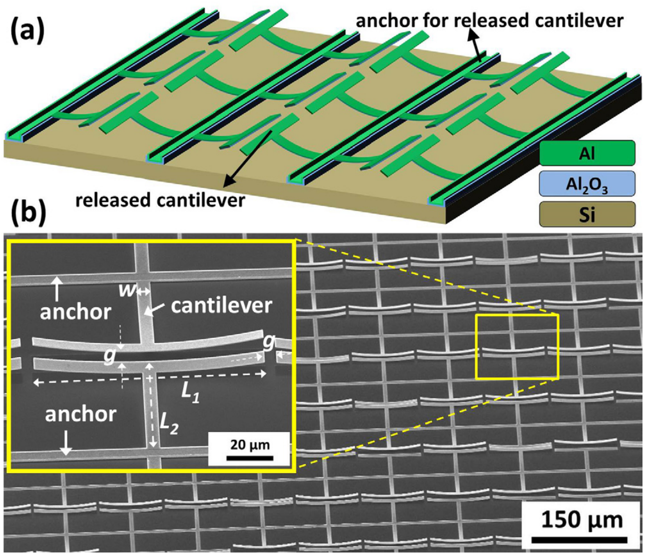

FIG. 1. (a) Schematic of the MTM device after released. (b) SEM image of MTM array. Inset shows the zoom-in SEM image of yellow square, where geometry parameters of the MTM are $L_1 = 100\,\mu$m, $L_2 = 50\,\mu$m, $w = 6\,\mu$m, and $g = 4\,\mu$m.

MTM array after the cantilevers are released and the corresponding geometric parameters. As seen from the zoom-in SEM image, the initial height of curving cantilever is $15\,\mu$m. This gap between the metamaterial and substrate is an important tuning parameter, since different configurations of the unit cell can be obtained by simply adjusting the gap value. When the driving voltage is increased, the cantilevers are attracted from the initial position toward the substrate. The deformation of the cantilevers is determined by the balance between the electrostatic force and the cantilever restoring force. When the voltage difference between the cantilevers and the substrate exceeds the critical voltage, known as the pull-in voltage, the cantilevers become unstable and pull onto the substrate. Hence, the resonant frequency can be actively and continuously controlled for applied voltages below the pull-in voltage.

The EM responses of MTM device were characterized by using THz-TDS in the transmission mode. The experiments were performed at room temperature in a nitrogen purged chamber. The measured and simulated transmission spectra of MTM device with TM and TE polarization incidences are shown in Fig. 2, respectively, as solid lines and circular symbols. The TM polarization state represents the case in which the electric field is parallel to the split side of the ring, while TE occurs when the electric field is perpendicular to the split side. Figures 2(a)–2(c) show the measured and simulated transmission spectra in the frequency range of 0–3 THz for the TM polarization incidence. The resonance is purely due to the electric field is oriented along a mirror plane for the T-shape structures. The resonant frequency is shifted from 0.65 THz to 0.92 THz compared to the device without driving voltage to 12 V DC bias, resulting in a tuning range of 0.27 THz. For TE polarization, there are two distinct resonances in the spectrum as shown in Figs. 2(d)–2(f). The lower resonant frequency is due to the inductive-capacitive (LC) resonance, where oscillating charges generate circulating currents throughout the entire structure and result in a pure electric response. The second resonant frequency is dipole-type electrical resonance, which originates from the excitation of electric dipoles.[31,32] The resonant frequencies are shifted by 0.37 THz and 0.50 THz for LC and dipolar resonances, respectively, in comparison to the device without DC bias and it is snapped down to Si substrate at 12 V DC bias. These results evidently show that the MTM device is polarization dependent for TM and TE polarization incidence.

Furthermore, we also investigated the flexibility of this device by using four kinds of liquids dropped on the snap-down device surface, respectively, that schematic is shown in Fig. 3(a) and exposed to atmospheric air in comparison to the chamber purged with N_2 gas. Under TE polarization, the transmission spectra for the various liquids are plotted in Fig. 3(b). There is a significant red-shift in the resonant frequency as the refractive index of the liquid covering the device increases. Additionally, the use of microfluidic channels

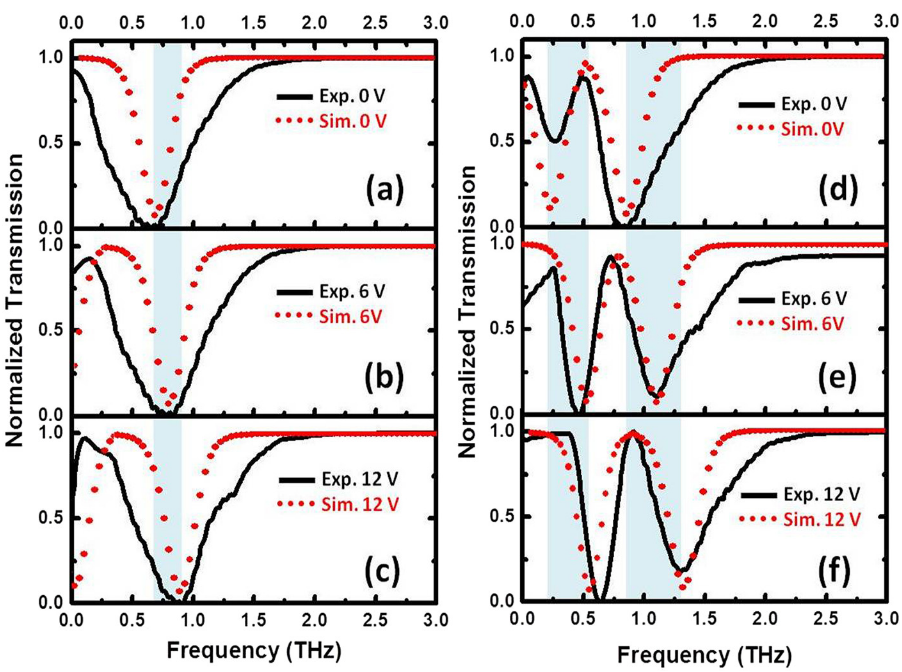

FIG. 2. The measured and simulated transmission spectra of the MTM device. (a)–(c) and (d)–(f) represent TM and TE polarization incidence, respectively. The circular symbols and solid lines show the numerically simulated and experimentally measured spectra of transmission, respectively. The shaded regions represent the shift of the resonant frequencies. The first, second, and third rows show the spectra, when the applied DC voltage is 0 V ((a), (d)), 6 V ((b), (e)), and 12 V ((c), (f)).

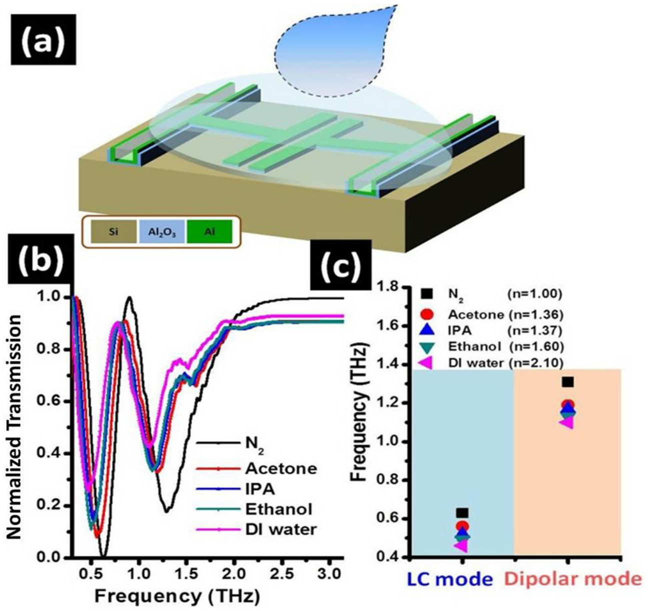

FIG. 3. (a) Schematic of a liquid droplet on the snap-down device surface. (b) The measured transmission spectra with respect to various liquids. (c) The resonant frequencies of MTM device at LC and dipolar resonances measured under various liquids.

exhibits numerous significant advantages for lab-on-chips applications, including well-behaved laminar flow, fast diffusion, low analytic consumption, and portability. In Fig. 3(b), the LC resonances for N_2, acetone, IPA, ethanol, and DI water are 0.63, 0.56, 0.52, 0.49, and 0.46 THz, respectively, and for dipolar resonances are 1.31, 1.19, 1.17, 1.13, and 1.10 THz, respectively. All the resonances are summarized in the Fig. 3(c), the resonant frequencies are shifted 0.17 and 0.21 THz, for LC and dipolar resonance, respectively.

To verify the flow tuning characteristic of MTM device, we prepared another MTM device encapsulated in a PDMS fluidic channel and characterized by using THz-TDS system. The schematic of experimental setup is shown in Fig. 4(a). Inlet and outlet of the PDMS fluidic channel are formed by having Tyron tubes inserted for sample delivery. The fluidic channel is connected to a syringe, via inlet tube, and syringe pump which is used to drive the sample and control the flow rate accurately. The flow tuning mechanism is used the difference in flow rate caused different forces acting on the MTM cantilevers. The major interaction between the liquid and the MTM cantilevers is considered as a stress field, producing a pressure along the flow direction, i.e., x-direction in Fig. 4(a) and a shear stress originating from the viscosity of the liquid. We assume the flow is steady and unidirectional. The liquid force can be expressed as[33]

$$\frac{\partial^2 u}{\partial z^2} + \frac{\partial^2 u}{\partial y^2} = \frac{1}{\mu}\frac{dP}{dx}, \tag{1}$$

where u is the velocity (m/s) of the liquid in the x-direction, μ is the dynamic viscosity (kg/(m s)) of the liquid, and dP/dx is the pressure gradient (Pa/m) along the x-direction. The solution for the x-component of the liquid velocity is solved and then integrated to find the relation between the volumetric flow rate and the pressure gradient, which yields the solution[33]

$$\frac{dP}{dx} = \frac{3\mu Q}{4wh^3 S}, \tag{2}$$

where Q is the volumetric flow rate (m^3/s), w and h are half of the height (m) and width (m) of the fluidic channel, respectively, and S is a factor depending on the geometry of the fluidic channel. Thus, the liquid force is proportional to the volumetric flow rate. Since the liquid under the cantilevers is assumed to be quiescent while the liquid flowed over the device, the pressure beneath the cantilevers is constant at the value of the free end as the pressure above the cantilevers continues to increase linearly in the upstream direction. This effect creates a varying force on the cantilevers surface and affects its deflection. The schematics of the forces deflect the MTM cantilevers at different bending state, respectively, are shown in Figs. 4(b)–4(d). According to the results of Fig. 3, we chose the liquids of larger different refraction index, i.e., acetone and DI water, for flow tuning characteristic of MTM. The device was measured under TE polarization by using THz-TDS system. The flow rate was controlled by a

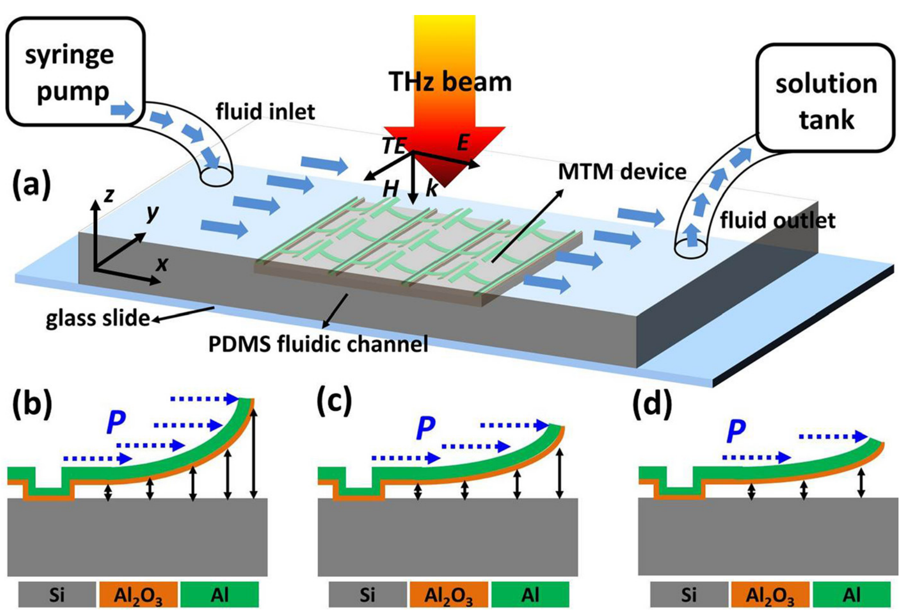

FIG. 4. (a) Schematic of the MTM device integrated with a PDMS fluidic channel. (b)–(d) present the initial, intermediate, and final state of a MTM cantilever with respect to low, medium, and high flow rate, respectively.

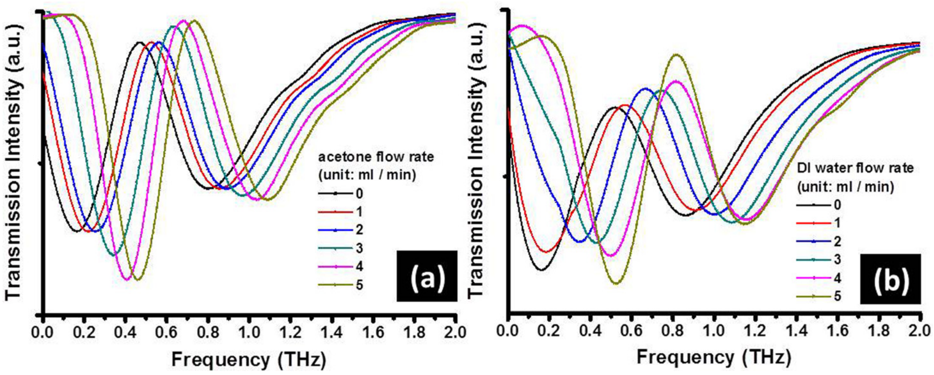

FIG. 5. The flow tuning characteristic of the MTM device measured by using THz-TDS under TE polarization. (a) Acetone and (b) DI water solutions were injected into PDMS fluidic channel at different flow rates ranging from 0 to 5 ml/min.

syringe pump, ranging from 0 to 5 ml/min per 1 ml/min step, respectively. Figure 5(a) shows the transmission spectra of MTM device actuated by acetone solution. The corresponding resonances of MTM device were measured as 0.15 THz (LC resonance) and 0.79 THz (dipolar resonance) for an empty channel, and 0.46 THz (LC resonance) and 1.09 THz (dipolar resonance) for acetone with 5 ml/min flow rate, respectively. In the case of DI water solution, the resonances were shifted from 0.16 THz to 0.52 THz (LC resonance) and 0.85 to 1.14 THz (dipolar resonance) for testing in an empty channel and 5 ml/min flow rate, respectively, as shown in Fig. 5(b). The variation range of these two kinds of liquids is 0.30 THz and the EM tunability of MTM controlled by different flow rates is linearly for comparison with 1–5 ml/min.

In conclusion, we have demonstrated a MTM device with active and continuous out-of-plane control by using either electrostatic force or liquid force pressure in the THz frequency range. When the device was actuated by electrostatic force, the tuning ranges of resonant frequency are 0.27 THz and 0.50 THz for TM and TE polarization incidence, respectively. When the snap-down device is covered with various liquid droplets, the experimental results indicate the feasibility of refractive index detection for different chemical solutions. As the flow tuning characteristic of MTM device integrated with a PDMS fluidic channel, the variation range of the resonant frequency is 0.30 THz versus the change of liquid flow rate from 0 to 5 ml/min. It indicates a creation of remote actuation mechanism of tunable THz metamaterials by using the liquid with different flow rate to adjust the bending degree of MTM cantilevers. With our experimental results, it is seen that out-of-plane metamaterial can be used as a flow sensor for arterial blood flow measurement. This in turn opens up opportunities for healthcare applications, notably implantable blood flow monitoring.

The authors acknowledge the financial support from research grant of MOE AcRF Tier 2 - MOE2012-T2-2-154 and Science and Engineering Research Council (SERC) grant 1220103064 from the Agency for Science, Technology and Research (A-STAR).

[1] J. B. Pendry, D. Schurig, and D. R. Smith, Science **312**, 1780–1782 (2006).
[2] N. I. Zheludev and Y. S. Kivshar, Nature Mater. **11**, 917 (2012).
[3] D. Shin, Y. Urzhumov, Y. Jung, G. Kang, S. Baek, M. Choi, H. Park, K. Kim, and D. R. Smith, Nat. Commun. **3**, 1213 (2012).
[4] N. Fang and X. Zhang, Appl. Phys. Lett. **82**, 161–163 (2003).
[5] N. I. Landy, S. Sajuyigbe, J. J. Mock, D. R. Smith, and W. J. Padilla, Phys. Rev. Lett. **100**, 207402 (2008).
[6] Y. C. Jun, J. Reno, T. Ribaudo, E. Shaner, J.-J. Greffet, S. Vassant, F. Marquier, M. Sinclair, and I. Brener, Nano Lett. **13**, 5391–5396 (2013).
[7] H.-T. Chen, W. J. Padilla, J. M. O. Zide, A. C. Gossard, A. J. Taylor, and R. D. Averitt, Nature **444**, 597–600 (2006).
[8] Z. Liu, C.-Y. Huang, H. Liu, X. Zhang, and C. Lee, Opt. Express **21**, 6519–6525 (2013).
[9] S. Savo, D. Shrekenhamer, and W. J. Padilla, Adv. Opt. Mater. **2**, 275–279 (2014).
[10] Y. Zhu, S. Vegesna, Y. Zhao, V. Kuryatkov, M. Holtz, Z. Fan, M. Saed, and A. A. Bernussi, Opt. Lett. **38**, 2382–2384 (2013).
[11] H. Tao, A. C. Strikwerda, K. Fan, W. J. Padilla, X. Zhang, and R. D. Averitt, Phys. Rev. Lett. **103**, 147401 (2009).
[12] R. Singh, A. K. Azad, Q. X. Jia, A. J. Taylor, and H.-T. Chen, Opt. Lett. **36**, 1230–1232 (2011).
[13] R. Singh, Z. Tian, J. Han, C. Rockstuhl, J. Gu, and W. Zhang, Appl. Phys. Lett. **96**, 071114 (2010).
[14] M. Gil, C. Damm, A. Giere, M. Sazegar, J. Bonache, R. Jakoby, and F. Martı′n, Electron. Lett. **45**, 417–418 (2009).
[15] D. R. Chowdhury, R. Singh, A. J. Taylor, H.-T. Chen, and A. K. Azad, Appl. Phys. Lett. **102**, 011122 (2013).
[16] K. Fan, A. C. Strikwerda, X. Zhang, and R. D. Averitt, Phys. Rev. B **87**, 161104(R) (2013).
[17] K. Fan, X. Zhao, J. Zhang, K. Geng, G. R. Keiser, H. R. Seren, G. D. Metcalfe, M. Wraback, X. Zhang, and R. D. Averitt, IEEE Trans. Terahertz Sci. Technol. **3**, 702–708 (2013).
[18] J. Han, A. Lakhtakia, and C.-W. Qiu, Opt. Express **16**, 14390–14396 (2008).
[19] W. M. Zhu, A. Q. Liu, X. M. Zhang, D. T. Tsai, T. Bourouina, J. H. Teng, X. H. Zhang, H. C. Guo, H. Tanoto, T. Mei, G. Q. Lo, and D. L. Kwong, Adv. Mater. **23**, 1792–1796 (2011).
[20] W. M. Zhu, A. Q. Liu, T. Bourouina, D. P. Tasi, J. H. Teng, X. H. Zhang, G. Q. Lo, D. L. Kwong, and N. I. Zheludev, Nat. Commun. **3**, 1274 (2012).
[21] Y. H. Fu, A. Q. Liu, W. M. Zhu, X. M. Zhang, D. P. Tsai, J. B. Zhang, T. Mei, J. F. Tao, H. C. Guo, X. H. Zhang, J. H. Teng, N. I. Zheludev, G. Q. Lo, and D. L. Kwong, Adv. Funct. Mater. **21**, 3589–3594 (2011).
[22] J. Y. Ou, E. Plum, J. Zhang, and N. I. Zheludev, Nat. Nanotechnol. **8**, 252–255 (2013).
[23] X. Liu and W. J. Padilla, Adv. Opt. Mater. **1**, 559–562 (2013).
[24] Y. S. Lin, Y. Qian, F. Ma, Z. Liu, P. Kropelnicki, and C. Lee, Appl. Phys. Lett. **102**, 111908 (2013).
[25] Y. S. Lin, F. Ma, and C. Lee, Opt. Lett. **38**, 3126–3128 (2013).
[26] F. Ma, Y. Qian, Y. S. Lin, H. Liu, X. Zhang, Z. Liu, J. M.-L. Tsai, and C. Lee, Appl. Phys. Lett. **102**, 161912 (2013).
[27] F. Ma, Y. S. Lin, X. Zhang, and C. Lee, Light Sci. Appl. **3**, e171 (2014).
[28] P. Pitchappa, C. P. Ho, Y. S. Lin, P. Kropelnicki, C. Y. Huang, N. Singh, and C. Lee, Appl. Phys. Lett. **104**, 151104 (2014).
[29] J. Y. Ou, E. Plum, L. Jiang, and N. I. Zheludev, Nano Lett. **11**, 2142–2144 (2011).
[30] C. P. Ho, P. Pitchappa, Y. S. Lin, C. Y. Huang, P. Kropelnicki, and C. Lee, Appl. Phys. Lett. **104**, 161104 (2014).
[31] H.-T. chen, J. F. O'Hara, A. J. Taylor, and R. D. Averitt, Opt. Express **15**, 1084–1095 (2007).
[32] W. J. Padilla, A. J. Taylor, and R. D. Averitt, Phys. Rev. Lett. **96**, 107401 (2006).
[33] M. A. Schmidt, R. T. Howe, S. D. Senturia, and J. H. Haritonidis, IEEE Trans. Electron Devices **35**, 750–757 (1988).